NANO EXPRESS

Open Access

CrossMark

The remanence ratio in CoFe$_2$O$_4$ nanoparticles with approximate single-domain sizes

Shitao Xu[1,2], Yongqing Ma[1*], Bingqian Geng[1], Xiao Sun[1] and Min Wang[1]

Abstract

Approximately single-domain-sized 9-, 13-, and 16-nm CoFe$_2$O$_4$ nanoparticles are synthesized using the thermal decomposition of a metal-organic salt. By means of dilution and reduction, the concentration, moment, and anisotropy of nanoparticles are changed and their influence on the magnetic properties is investigated. The relation of $M_r/M_s \propto 1/lgH_{dip}$ is observed, where M_r/M_s is the remanence ratio and H_{dip} is the maximum dipolar field. Especially, such relation is more accurate for the nanoparticle systems with higher concentration and higher moment, i.e., larger H_{dip}. The deviation from $M_r/M_s \propto 1/lgH_{dip}$ appearing at low temperatures can be attributed to the effects of surface spins for the single-phase CoFe$_2$O$_4$ nanoparticles and to the pinning effect of CoFe$_2$O$_4$ on CoFe$_2$ for the slightly reduced nanoparticles.

Keywords: CoFe$_2$O$_4$ nanoparticles, Remanence ratio, Dipolar interaction, Surface spins

Background

Nanoscale magnetic materials often exhibit novel properties, differing from those of their bulk polycrystalline counterparts [1–5], as a result of several effects including the finite size effect, surface effect, and interparticle interaction [6–8]. These effects affect the magnetic properties and the magnetic ordering state of nanoparticles (NPs) individually, and sometimes synergetically which usually occurs in the dense magnetic NPs. One typical phenomenon of the size effect is that the coercivity (H_c) reaches the maximum as the particle size (D) decreases to a single-domain critical dimension D_c, and then reduces monotonically to zero when D is further decreased to a certain size below D_c [9]. Concomitantly, the NPs exhibit the superparamagnetic behavior with the theoretical remanence (M_r) to saturation (M_s) magnetization ratio (M_r/M_s) being zero. Surface spin is another factor to affect the magnetic properties for the nano-sized magnetic materials. The total magnetization of a nanoparticle composes of the surface and core spins [10, 11], which is known as the core-shell magnetization model. Surface spins reduce the magnetization of a magnetic nanoparticle due to the disorder of spins at the nanoparticle surface, and the disordered surface spins lower the critical magnetic ordering temperature of magnetic nanoparticles compared with that of the bulk material [12]. Below a certain temperature, the canted surface spins freeze into a spin-glass-like state and the hysteresis loops obtained after a field cooling (FC) shift, as a consequence of the unidirectional anisotropy resulting from the coupling between the disordered surface layer and core spins [6, 13, 14]. Furthermore, the interaction between the surface spins of different particles enhances the effective anisotropy [7, 15], making the surface anisotropy constant many orders higher than that of the bulk material [16].

Apart from surface spins, the interparticle dipolar interaction (IPDI) widely exists in the magnetic NPs; it plays a complex role in magnetic properties. For example, it has been suggested that the IPDI enhances H_c because of additional induced anisotropy [17], while the opposite conclusion has also been observed [18]. A strong IPDI decreases the M_r/M_s ratio, which has been proved both theoretically and experimentally [18–23]. Furthermore, it is well known that the strength of IPDI depends on the concentration of magnetic NPs and

* Correspondence: yqma@ahu.edu.cn
[1]Anhui Key Laboratory of Information Materials and Devices, School of Physics and Materials Science, Anhui University, Hefei 230601, People's Republic of China
Full list of author information is available at the end of the article

Xu *et al. Nanoscale Research Letters* (2016) 11:471

Page 2 of 9

obviously affects the magnetic ordering states: in a heavily diluted system with low concentration of magnetic NPs, the system exhibits superparamagnetism [24], while in a dense system with high concentration, the NPs exhibit the super-spin glass (SSG) states at low temperature [25, 26].

So far, the effects of IPDI on the magnetic properties have not been comprehensively investigated, instead they have been reported piecemeal by different researchers. The strength of IPDI, which can be expressed by the maximum dipolar field H_{dip}, defined as $H_{dip} = 2\,\mu/d^3$, where μ is the particle moment ($\mu = M_s \times V_m$; M_s is saturation magnetization and V_m is magnetic grain volume) and d is the distance between particles (center to center), which is inversely proportional to the NP concentration. The purpose of the present work is to systematically reveal the effects of H_{dip} on the M_r/M_s ratio for the 9-, 13-, and 16-nm magnetic NPs with different concentrations, particle moments, and anisotropies.

Methods
Experimental Procedure
Preparation of CoFe$_2$O$_4$ NPs
Co(acac)$_2$ (97 %; acac is acetylacetonate), Fe(acac)$_3$ (98 %), benzyl ether (97 %), oleic acid (90 %), and oleylamine (80–90 %) were mixed in a 1000-ml three-necked round-bottom flask by magnetic stirring under a flow of nitrogen (99.999 %). The mixture was heated at 120 °C for 0.5 h to remove air and moisture, at 200 °C under reflux for 2 h, and then at 290 °C for 1 h. After the mixture was cooled naturally to room temperature, absolute ethanol was added to produce a precipitate. The precipitate was separated via centrifugation and then washed with absolute ethanol several times to obtain CoFe$_2$O$_4$ NPs. By varying the intermediately treating temperature, we prepared 9-, 13-, and 16-nm CoFe$_2$O$_4$ NPs.

Dilution of CoFe$_2$O$_4$ NPs in a SiO$_2$ Matrix
In order to change the interparticle distance, some of the 9- and 13-nm CoFe$_2$O$_4$ NPs were diluted in a SiO$_2$ matrix with different concentrations, because the interparticle distance is inversely proportional to the concentration. CoFe$_2$O$_4$ NPs were added to a solution of cyclohexane (400 ml), polyethylene glycol (25 ml), tetraethyl orthosilicate, and ammonia, and then stirred mechanically for 24 h. Ethanol was added to form a precipitate. The precipitate was isolated by centrifugation and then washed with ethanol and water to remove unreacted molecules. The precipitate was dried at 80 °C for 6 h to obtain the diluted CoFe$_2$O$_4$ NPs by SiO$_2$. By increasing the relative content of CoFe$_2$O$_4$, we prepared the CoFe$_2$O$_4$ NPs with low, moderate, and high concentrations, and the samples

are referred to as L9, M9, and H9 for 9-nm NPs and as L13, M13, and H13 for 13-nm NPs.

Reduction of CoFe$_2$O$_4$ NPs
In order to change the moment and anisotropy of NPs, the reduction reactions were performed in the H$_2$/N$_2$ atmosphere (500 sccm, 96 % N$_2$ + 4 % H$_2$) to prepare a composite of CoFe$_2$O$_4$ and CoFe$_2$ alloy, because the CoFe$_2$ alloy is a typical soft ferromagnet with high moment and small anisotropy, compared with CoFe$_2$O$_4$. To avoid the aggregation of NPs during reduction, the 16-nm NPs were first diluted or separated by SiO$_2$ and then reduced at low, moderate, and high temperatures at 300, 400, and 500 °C for 4 h, and the obtained samples are denoted as LT16, MT16, and HT16.

Characterization
The crystal structure of the products was determined by X-ray diffraction (XRD) using an X-ray diffractometer (DX-2000 SSC) with Cu Kα irradiation ($\lambda = 1.5406$ Å) in the scanning range 20°–80° with a step size of 0.02°. (High-resolution) transmission electron microscopy ((HR)TEM; JEOL, JEM-2100) was used to observe the morphology characteristics. Magnetic measurements were carried out using a superconducting quantum interference device PPMS system (Quantum Design, PPMS EC-II).

Results and Discussion
Crystal Structure and Morphology
TEM images and size histograms in Fig. 1 show that the NPs are ca. 9, 13, and 16 nm. Most of 9- and 13-nm NPs exhibit the spherical-like morphology, while some 16-nm NPs exhibit rhombohedral and quadrate shapes. The size distribution range is ca. 2 nm for the 9-nm NPs and 4 nm for 13- and 16-nm NPs.

The XRD experiments have been performed on all samples, and herein, we show the results of several samples representatively. As shown in Fig. 2b–d, the as-prepared and undiluted 9-nm (the H9 sample), 13-nm (the H13 sample), and 16-nm CoFe$_2$O$_4$ NPs are single phases and have the cubic spinel structure, according to the standard powder diffraction file (PDF) of CoFe$_2$O$_4$ (No. 22-1086) in Fig. 2a. For the diluted 16-nm NPs after reduction at 400 °C, i.e., the MT16 sample, the extra diffraction peaks, besides those from CoFe$_2$O$_4$, can be assigned to the reflection from (110) and (200) crystallographic planes of the CoFe$_2$ alloy, according to the PDF card of CoFe$_2$ (No. 65-4131) in Fig. 2f. This XRD result indicates that CoFe$_2$O$_4$ is partially reduced to CoFe$_2$ due to the reaction: CoFe$_2$O$_4$ + 4H$_2$ → CoFe$_2$ + 4H$_2$O [27]. To observe the existence of CoFe$_2$ in the reduced sample, the (HR)TEM was ever performed on the undiluted

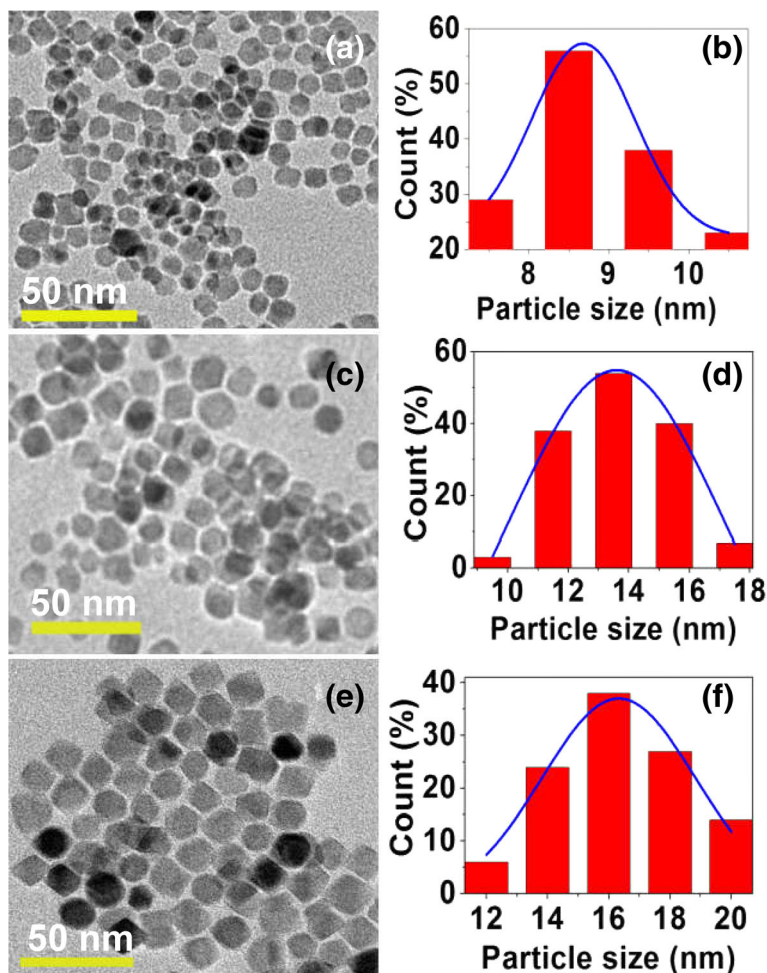Xu et al. Nanoscale Research Letters (2016) 11:471

Page 3 of 9

Fig. 1 TEM images (*left*) and size distribution histograms with Gaussian-fitteng curve (*solid line*) (*right*) for 9-nm (**a** and **b**), 13-nm (**c** and **d**) and 16-nm (**e** and **f**) CoFe$_2$O$_4$ NPs

sample. The lattice fringes of CoFe$_2$ can be observed at the surface of particle, i.e., CoFe$_2$ exists at the outer layer while CoFe$_2$O$_4$ exists in the inner of particle.

Magnetic Properties

The dependence of the magnetization (M) of all samples on the applied magnetic field (H), i.e., $M(H)$ loop ($-70 \ \text{kOe} < H < 70 \ \text{kOe}$) was measured at temperatures of 10, 50, 100, 150, 200, 250, 300, and 390 K. Representatively, the $M(H)$ loops recorded at 10 and 390 K were shown in Fig. 3 for 9- and 13-nm NPs with different concentrations and in Fig. 4 for diluted 16-nm NPs with different reducing temperatures. From these loops, the coercivity (H_c), saturation magnetization (M_s), and remanence (M_r) to saturation magnetization ratio (M_r/M_s) values at different temperatures can be obtained. In the case of the CoFe$_2$O$_4$ NPs with moderate (Fig. 3b, e) and high (Fig. 3c, f)

concentrations, the loops recorded at 10 K show a jump around $H = 0$; this phenomenon is common for magnetic NPs and can be assigned to the reorientation of surface spins around NPs [28, 29]. However, in the case of the CoFe$_2$O$_4$ NPs with low concentration, as shown in Fig. 3a, d, the 10-K loops become smooth which is characteristic of a single-phase hard magnet, and the possible reason is that the surface spins are strongly pinned by the SiO$_2$ matrix.

For the diluted and reduced 16-nm NPs, containing CoFe$_2$O$_4$ and CoFe$_2$ phases, as shown in Fig. 4, the jump around $H = 0$ becomes higher as the reducing temperature increases, as a result of the increase in the relative CoFe$_2$ content [30, 31]. Herein, the jump is attributable to the different reversal fields of hard CoFe$_2$O$_4$ and soft CoFe$_2$, which is an indicative of no exchange-coupling occurring between soft and hard species, because in an exchange-coupled system, the magnetization could show an equivalent reversal
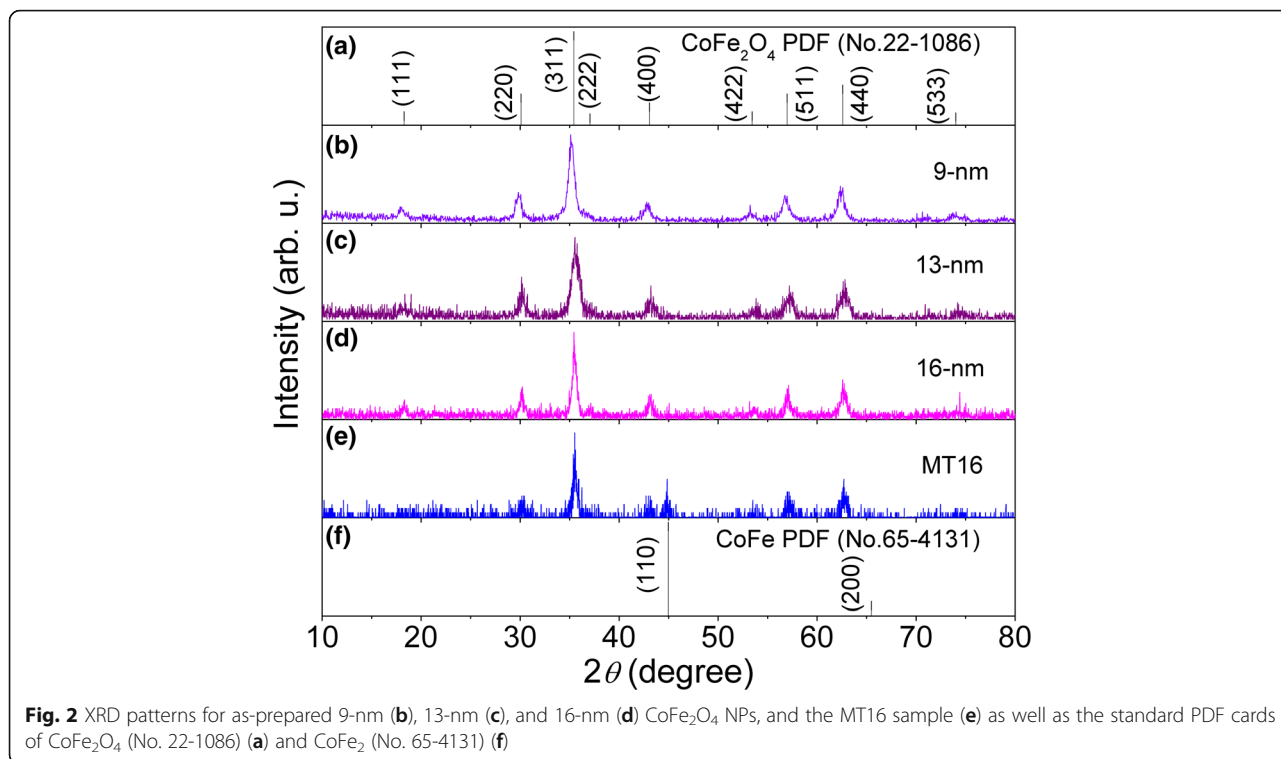
Xu *et al. Nanoscale Research Letters* (2016) 11:471

Page 4 of 9

Fig. 2 XRD patterns for as-prepared 9-nm (**b**), 13-nm (**c**), and 16-nm (**d**) CoFe$_2$O$_4$ NPs, and the MT16 sample (**e**) as well as the standard PDF cards of CoFe$_2$O$_4$ (No. 22-1086) (**a**) and CoFe$_2$ (No. 65-4131) (**f**)
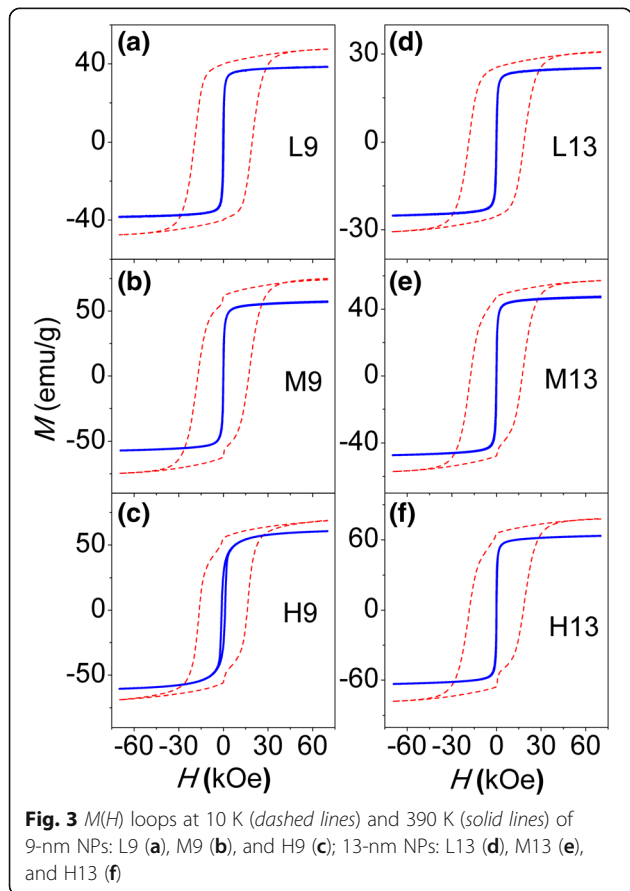

Fig. 3 *M(H)* loops at 10 K (*dashed lines*) and 390 K (*solid lines*) of 9-nm NPs: L9 (**a**), M9 (**b**), and H9 (**c**); 13-nm NPs: L13 (**d**), M13 (**e**), and H13 (**f**)

behavior over the whole temperature region and the loop should be as smooth as that of the single-phase hard magnet. With increasing temperature, the anisotropy field of CoFe$_2$O$_4$ decreases markedly, so the average reversal fields of hard and soft phases may be similar, resulting in the single-phase behavior of the loops (not shown here).

The undiluted 9- and 13-nm NPs, i.e., H9 and H13, as well as the 16-nm NPs reduced at 300 °C (LT16) have the H_c values of 20.0, 18.8, and 20.5 kOe at 10 K, smaller than 23.8 kOe (10 K) for our previously reported 10.7-nm CoFe$_2$O$_4$ NPs [32] which particle size is close to the critical size of a single domain [33]. These H_c values are much larger than that for the bulk CoFe$_2$O$_4$ (6.8 kOe at 10 K) [34], because on the one hand, the particles are approximately single-domain sized, and on the other hand, the interaction between surface spins induces extra anisotropy and hence enhances H_c, which will be further discussed below. As the temperature increases, H_c monotonically decreases. The decrease in coercivity can be attributable to thermal fluctuations of the blocked moment, across the anisotropy barrier. For an assembly of non-interacting single-domain magnetic nanoparticles with uniaxial anisotropy, the coercivity can be written in the form of simple model of thermal activation of particle moments over the anisotropy barriers (Kneller's law) as [6, 35] $H_c = H_{c0}[1 - (T/T_B)^{1/2}]$, where H_{c0} is the value of H_c at 0 K and T_B denotes the blocking temperature. The H_c
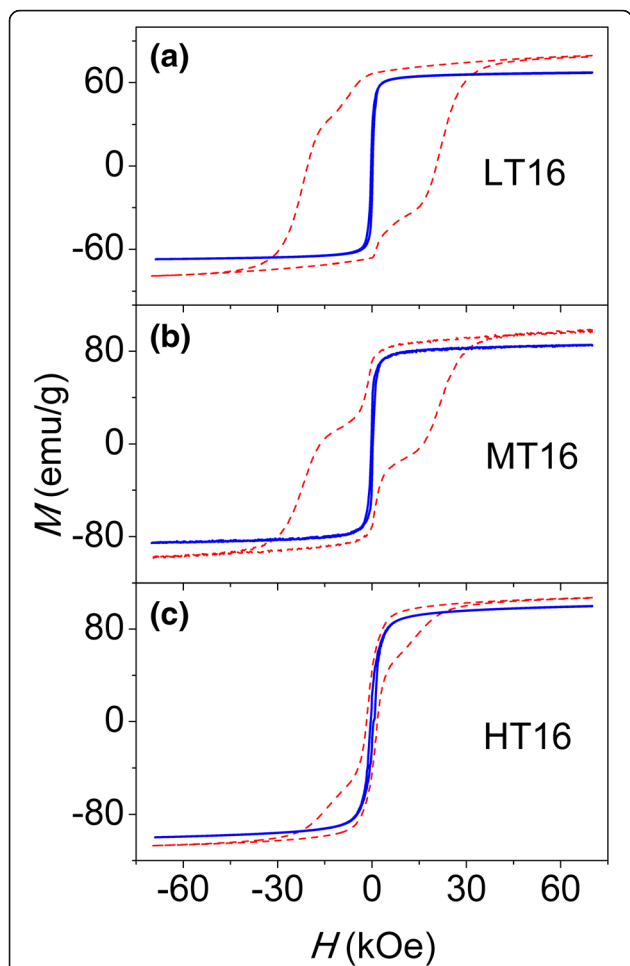
Xu et al. Nanoscale Research Letters (2016) 11:471

Page 5 of 9

Fig. 4 $M(H)$ loops of diluted 16-nm NPs with low, moderate, and high reducing temperatures, i.e., LT16 (**a**), MT16 (**b**), and HT16 (**c**)
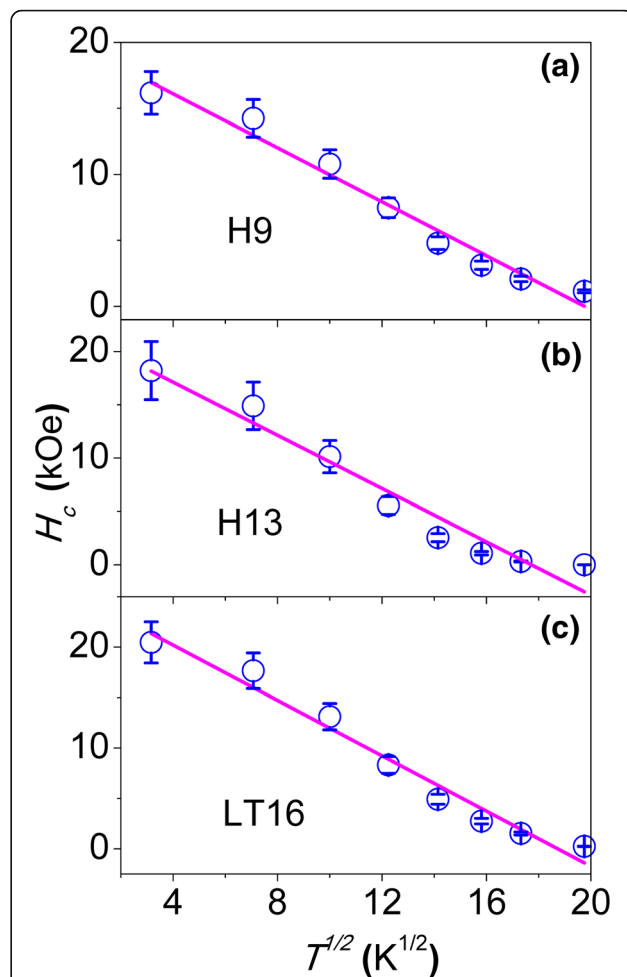

Fig. 5 Coercivity H_c versus square root temperature for samples (circles) H9 (**a**), H13 (**b**), and LT16 (**c**) where the solid line is the fit to the experimental data points according to Kneller's law

values of all samples can be fitted to Kneller's law in the temperature range of 10–390 K. Representatively, the experimental (solid circles) and fitting curves (solid lines) of the samples H9 (a), H13(b), and LT300 (c) are plotted in Fig. 5. The obtained fitting parameter T_B will be used to calculate the volume of magnetic grain, V_m, as discussed below.

In the case of non-interacting and randomly oriented spherical particles with cubic anisotropy, H_c obeys the relation of $H_c = 0.64 K/M_s$ [15], where K is the anisotropy constant, so the K value can be calculated for all samples. The highest K for $CoFe_2O_4$ NPs at 10 K reaches $\sim 10^7$ erg/cm^3, much larger than 1.8–3.0×10^6 erg/cm^3 for the bulk $CoFe_2O_4$; this is consistent with the previous reports that in thin films and nanoparticles, surface anisotropy constant is found higher by many orders of magnitude than that of the bulk [15, 16]. In narue the enhanced K value results from the interaction between the surface spins of different particles

[7], and between the spins from the surface and core in a single NP [6, 13]. Large K value induced by the surface spins leads to the increase of H_c due to $H_c \propto K$. It should be mentioned that the fitting according to Kneller's law and the calculation of K from $H_c = 0.64 K/M_s$ are based on an assumption that nanoparticles do not interact with each other. The real situation is that the dipolar interaction widely exists in the system of magnetic nanoparticles; however, the dipolar interaction is weak, compared with the anisotropy. Therefore, such the assumption has usually been considered to be reasonable in many previous reports [6, 15, 35].

Given T_B and K, the magnetic grain sizes (V_m) of the nanoparticles can be estimated according to Stoner-Wohlfarth expression [36]: $25k_B T_B = K V_m$, where k_B is the Boltzmann constant. Subsequently, the diameter D_m of a magnetic grain for all samples can be obtained, as shown in Fig. 6.
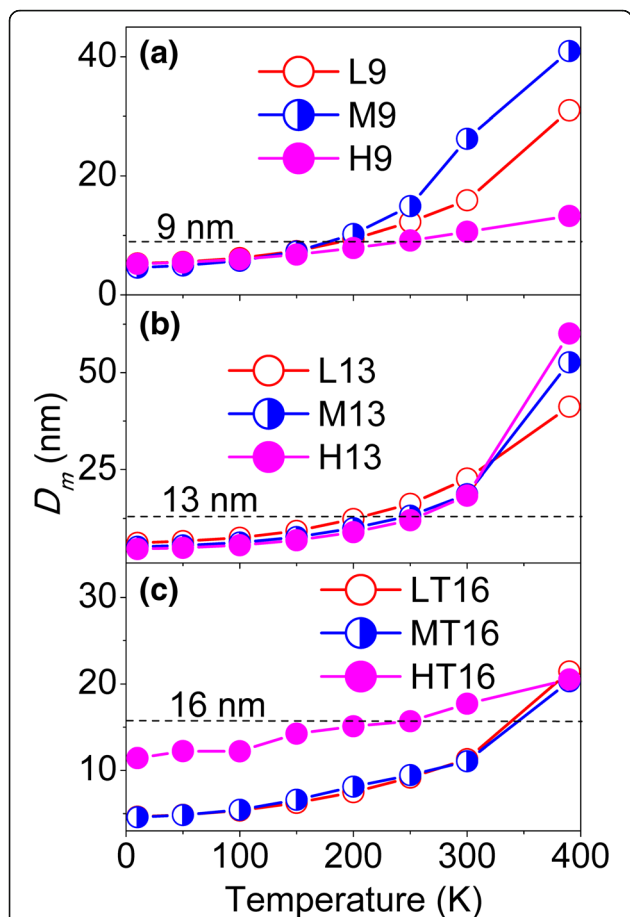
Xu et al. Nanoscale Research Letters (2016) 11:471

Page 6 of 9

Fig. 6 Magnetic grain size D_m at different temperatures of the diluted 9-nm (**a**) and 13-nm (**b**) NPs, diluted and reduced 16-nm (**c**) NPs

Fig. 7 The plot of the $1/\lg H_{dip}$ values and M_r/M_s ratios with added error bars (5 %) against temperature for diluted 9-nm NPs: L9 (**a**), M9 (**b**), and H9 (**c**)

The D_m values of the 9- and 13-nm NPs are smaller than D_{TEM} below about 250 K, because of the canted surface spin layer surrounding magnetic particles [37]. Above this temperature, D_m becomes larger than D_{TEM} because the surface spins become able to thermally fluctuate, so they can be polarized by the core moments [38]. Subsequently, the collective behavior of several particle moments promoted by the IPDI leads to an increase of D_m [28]. In the case of the diluted and reduced 16-nm NPs, D_m of the HT16 sample is much larger than that for the LT16 and MT16 samples as a result of the increase of strong magnetic CoFe$_2$.

Based on the obtained V_m values, the strength of IPDI can be estimated by calculating H_{dip} according to $H_{dip} = 2\mu/d^3$, where μ is the particle moment ($\mu = M_s \times V_m$; M_s is saturation magnetization and V_m is magnetic grain volume). The inverse of the logarithm of H_{dip}, i.e., $1/\lg H_{dip}$ values and M_r/M_s ratios with added error bars (5 %) are plotted against temperature (T) in Figs. 7, 8, and 9 for 9-, 13-, and 16-nm NPs, respectively.
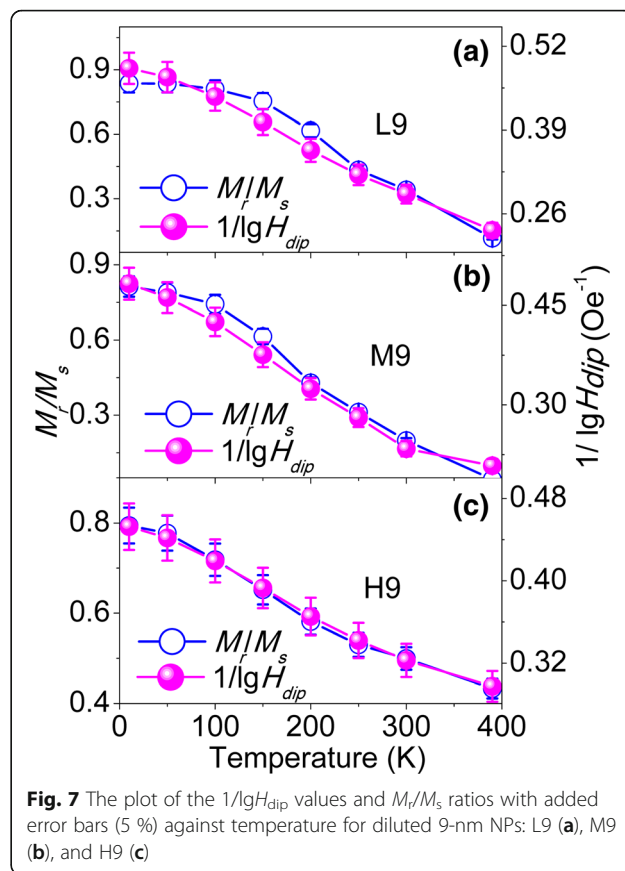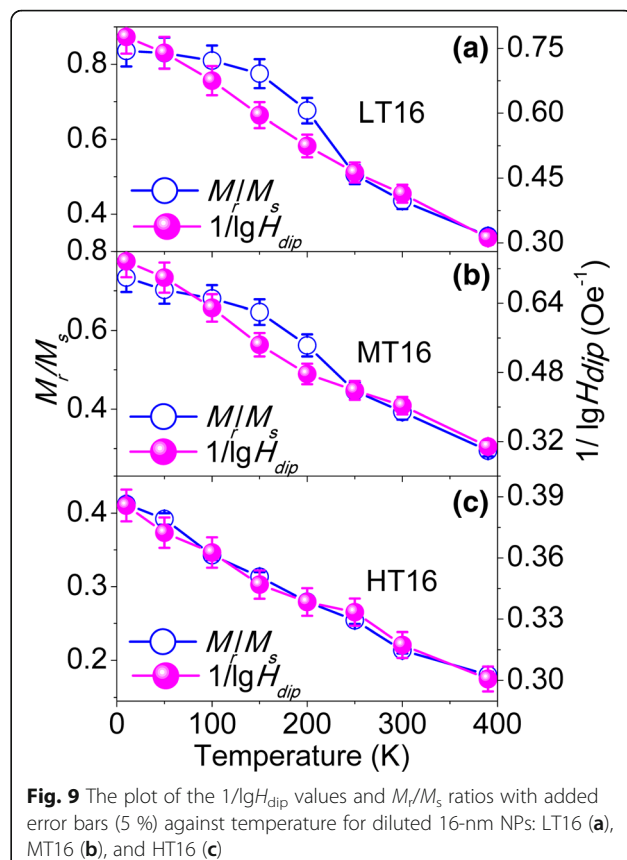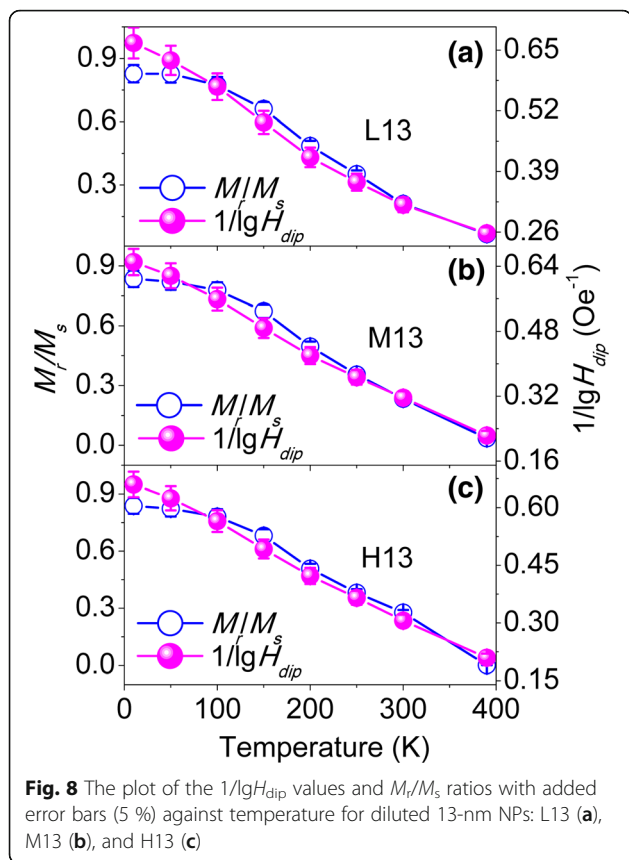
Next, we will discuss the correlation between M_r/M_s and H_{dip}. As seen in Figs. 7 and 8, the correlation between M_r/M_s and $1/\lg H_{dip}$ roughly follows $M_r/M_s \propto 1/\lg H_{dip}$ within a reasonable error range for 9- and 13-nm NPs, even though the NPs have different size and concentration. It can be noticed from Figs. 7 and 8 that the slope of the M_r/M_s curve is smaller than that for the $1/\lg H_{dip}$ curve at low temperatures, resulting in the deviation between M_r/M_s and $1/\lg H_{dip}$, which may result from the several competing effects, including the surface effects, finite size effects, and interparticle interactions, that are sometimes difficult to isolate in these nanoparticles, as suggested by Maaz [6]. As discussed in Fig. 6, the surface spins exist around the NP at low temperatures. Therefore, it is reasonable to suggest that the smaller slope of M_r/M_s may originate from the interaction between spins of surface and core and between surface spins of the neighboring particles.

In the case of the diluted and reduced 16-nm NPs which contain CoFe$_2$O$_4$ and CoFe$_2$, as seen in Fig. 9, the obvious deviation between M_r/M_s and $1/\lg H_{dip}$ for the slightly reduced LT16 and MT16, while M_r/M_s matches well with $1/\lg H_{dip}$ for the heavily reduced HT16, which can be assigned to the interaction in

Xu *et al. Nanoscale Research Letters* (2016) 11:471

Page 7 of 9

Fig. 8 The plot of the $1/\lg H_{\text{dip}}$ values and M_r/M_s ratios with added error bars (5 %) against temperature for diluted 13-nm NPs: L13 (**a**), M13 (**b**), and H13 (**c**)

Fig. 9 The plot of the $1/\lg H_{\text{dip}}$ values and M_r/M_s ratios with added error bars (5 %) against temperature for diluted 16-nm NPs: LT16 (**a**), MT16 (**b**), and HT16 (**c**)

$CoFe_2O_4/CoFe_2$ NPs. The interactions in $CoFe_2O_4/CoFe_2$ NPs occur at the interface (intraparticle) of $CoFe_2O_4$ and $CoFe_2$ and from the contact between NPs (interparticle). $CoFe_2O_4$ has a large magnetic anisotropy, so that it can exert a pinning action on the $CoFe_2$ phase, similar to the pinning effect of Fe oxide on Fe in Fe/Fe oxide NPs [38], which is the possible reason for the deviation between M_r/M_s and $1/\lg H_{\text{dip}}$. This suggestion may be supported by the results of the irreversible magnetization reversal field (H_{irr}) [27], defined as the magnetic field where the derivative (dM/dH) of the virgin curve has a peak. Figure 10 shows the field derivative dM/dH of the virgin curves for LT16 (a), MT16 (b), and HT16 (c) samples at 10 K. Two peaks locate at $H_{\text{irr}} = 7.90$ and 22.46 kOe for the LT16 sample, at $H_{\text{irr}} = 2.28$ and 22.60 kOe for the MT16 sample, and at $H_{\text{irr}} = 1.75$ and 11.70 kOe for the HT16 sample. The lower field corresponds to H_{irr} of $CoFe_2$, because pure $CoFe_2$ is a typical soft magnet and its H_{irr} is about 0.9 kOe at 10 K (not shown here), while the higher field corresponds to H_{irr} of hard $CoFe_2O_4$. The LT16 sample contains more $CoFe_2O_4$ and less $CoFe_2$, and $CoFe_2O_4$ exerts the pinning effect on the moment of $CoFe_2$, leading

to the highest H_{irr} of $CoFe_2$ among three samples. With increasing the reduction temperature, the sample contains more $CoFe_2$, and therefore the moment of $CoFe_2$ cannot be fully pinned by $CoFe_2O_4$, leading to the lower H_{irr} of $CoFe_2$ for the samples MT16 and HT16. Possibly, more $CoFe_2$ in HT16 polarizes the moments of $CoFe_2O_4$, resulting in the smaller H_{irr} of $CoFe_2O_4$ than that of LT16 [38]. These interactions in $CoFe_2O_4/CoFe_2$ NPs affect the moment reversal and consequently affect the M_r/M_s ratio.

However, compared with LT16 and MT16, the heavily reduced HT16 has the higher $CoFe_2$ content as a result of reduction at a higher temperature 500 °C. Therefore, HT16 has larger particle moment, and hence stronger interparticle dipolar interaction which overcomes other effects such as surface spins and interaction between $CoFe_2O_4$ and $CoFe_2$, consequently making the correlation between M_r/M_s and $1/\lg H_{\text{dip}}$ obey $M_r/M_s \propto 1/\lg H_{\text{dip}}$.

Conclusions
Well-dispersed uniform $CoFe_2O_4$ NPs with sizes of 9-, 13-, and 16-nm were synthesized. Some 9- and 13-nm NPs were diluted in a SiO_2 matrix to change their
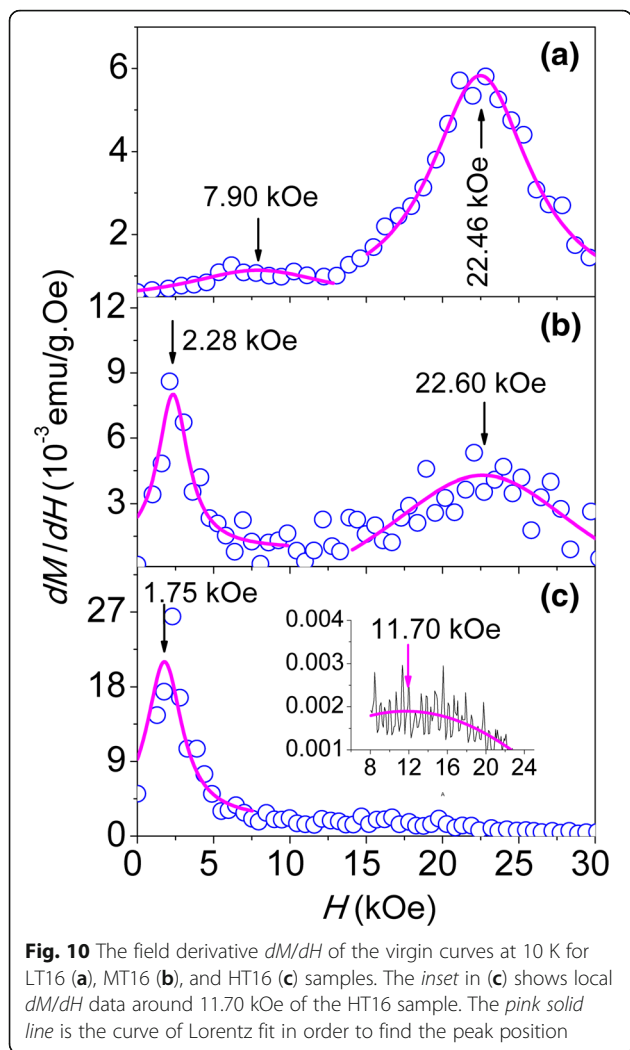
Xu *et al. Nanoscale Research Letters* (2016) 11:471

Page 8 of 9

Fig. 10 The field derivative *dM/dH* of the virgin curves at 10 K for LT16 (**a**), MT16 (**b**), and HT16 (**c**) samples. The *inset* in (**c**) shows local *dM/dH* data around 11.70 kOe of the HT16 sample. The *pink solid line* is the curve of Lorentz fit in order to find the peak position

concentration that is inversely proportional to interparticle distance, and some diluted 16-nm NPs were reduced by H_2 at 300, 400, and 500 °C to change the moment and anisotropy of the NPs. These samples were used as model systems to reveal the intrinsic correlation between M_r/M_s and IPDI, the strength of which was estimated by H_{dip}.

For the diluted 9- and 13-nm NPs that were not reduced, the correlation between M_r/M_s and H_{dip} follows $M_r/M_s \propto 1/lg\, H_{dip}$, regardless of the particle size and distance. Slight deviation from $M_r/M_s \propto 1/lg\, H_{dip}$, occurring at low temperatures, can be attributed to the effects of surface spins. In the case of the diluted and reduced 16-nm NPs, the relation between M_r/M_s and H_{dip} deviates $M_r/M_s \propto 1/lgH_{dip}$ for the slightly reduced NPs at 300 and 400 °C because of the pinning effect of $CoFe_2O_4$ on $CoFe_2$. However, the heavily reduced NPs at 500 °C follows $M_r/M_s \propto 1/lg\, H_{dip}$ because the strong interparticle dipolar interaction is a dominant factor to affect M_r/M_s.

Authors' Contributions
The manuscript was written through the contributions of all authors. The experiments and characterization were performed by STX, BQG, XS and MW. All of the tests were measured by STX. YQM contributed through research guidance, discussion, and manuscript modifications. All authors read and approved the final manuscript.

Competing Interests
The authors declare that they have no competing interests.

Author details
[1]Anhui Key Laboratory of Information Materials and Devices, School of Physics and Materials Science, Anhui University, Hefei 230601, People's Republic of China. [2]School of Physics and Electronic Information, Huaibei Normal University, Huaibei 235000, People's Republic of China.

References
1. Liang YC, Hsia HY (2013) Growth and crystallographic feature-dependent characterization of spinel zinc ferrite thin films by RF sputtering. Nanoscale Res Lett 8:537, pp8
2. Li XH, Xu CL, Han XH, Qiao L, Wang T, Li FS (2010) Synthesis and magnetic properties of nearly monodisperse $CoFe_2O_4$ nanoparticles through a simple hydrothermal condition. Nanoscale Res Lett 5:1039–1044
3. Martha SC, Martínez-Luévanos A, García-Cerda LA, Rodríguez-Fernández OS, Fuentes AF, Romero-García J, Montemayor SM (2015) Montemayor, nanostructured pure and substituted cobalt ferrites: fabrication by electrospinning and study of their magnetic properties. J Alloy Compd 653: 290–297
4. Du DJ, Yue WB, Ren Y, Yang XJ (2014) Fabrication of graphene-encapsulated $CoO/CoFe_2O_4$ composites derived from layered double hydroxides and their application as anode materials for lithium-ion batteries. J Mater Sci 49:8031–8039
5. Jiang CP, Leung CW, Pong PWT (2016) Magnetic-field-assisted assembly of anisotropic superstructures by iron oxide nanoparticles and their enhanced magnetism. Nanoscale Res Lett 11:189
6. Mazz K, Usman M, Karim S, Mumtaz A, Hasanain SK, Bertino MFJ (2001) Magnetic response of core-shell cobalt ferrite nanoparticles at low temperature. J Appl Phys 105:13917
7. Blanco-Gutierrez V, Virumbrales M, Saez-Puche R, Maria J (2013) Superparamagnetic behavior of MFe_2O_4 nanoparticles and MFe_2O_4/SiO_2 composites (M: Co, Ni). J Phys Chem C 117:20927–20935
8. Ji JY, Shih PH, Chan TS, Ma YR, Wu SY (2015) Magnetic properties of cluster glassy Ni/NiO core–shell nanoparticles: an investigation of their static and dynamic magnetization. Nanoscale Res Lett 10:243
9. Avazpour L, Khajeh MAZ, Toroghinejad MR, Shokrollahi H (2015) Synthesis of single-phase cobalt ferrite nanoparticles via a novel EDTA/EG precursor-based route and their magnetic properties. J Alloy Compd 637:497–503
10. Obaidat IM, Mohite V, Issa B, Tit N, Haik Y (2009) Predicting a major role of surface spins in the magnetic properties of ferrite nanoparticles. Cryst Res Technol 44(5):489–494
11. Xu ST, Ma YQ, Xu YF, Sun X, Geng BQ, Zheng GH, Dai ZX (2014) The effects of surface spin on magnetic properties of weak magnetic $ZnLa_{0.02}Fe_{1.98}O_4$ nanoparticles. Nanoscale Res Lett 9:545
12. Jing PP, Du JL, Jin CD, Wang JB, Pan LN, Li JN, Liu QF (2016) Improved coercivity and considerable saturation magnetization of cobalt ferrite ($CoFe_2O_4$) nanoribbons synthesized by electrospinning. J Mater Sci 51:885–892
13. Ceylan A, Hasanain SK, Shah SI (2008) Experimental observations of field-dependent activation of core and surface spins in Ni-ferrite nanoparticles. J Phys Condens Matter 20:195208

Xu et al. Nanoscale Research Letters (2016) 11:471

Page 9 of 9

14. Peddis D, Cannas C, Piccaluga G, Agostinelli E, Fiorani D (2010) Spin-glass-like freezing and enhanced magnetization in ultra-small $CoFe_2O_4$ nanoparticles. Nanotechnology 21:125705

15. Laureti S, Varvaro G, Testa AM, Fiorani D, Agostinelli E, Piccaluga G, Musinu A, Ardu A, Peddis D (2011) Magnetic interactions in silica coated nanoporous assemblies of $CoFe_2O_4$ nanoparticles with cubic magnetic anisotropy. Nanotechnology 21:315701

16. Prado Y, Mazerat S, Rivière E, Rogez G, Gloter A, Stéphan O, Catala L, Mallah T (2014) Magnetization reversal in $CsNi^{II}Cr^{III}(CN)_6$ coordination nanoparticles: unravelling surface anisotropy and dipolar interaction effects. Adv Funct Mater 24:5402–5411

17. Ewerlin M, Demirbas D, Brüssing F, Petracic O, Ünal AA, Valencia S, Kronast F, Zabel H (2013) Magnetic dipole and higher pole interaction on a square lattice. Phys Rev Lett 110:177209

18. Woinska M, Szczytko J, Majhofer A, Gosk J, Dziatkowski K, Twardowski A (2013) Magnetic interactions in an ensemble of cubic nanoparticles: a Monte Carlo study. Phys Rev B 88:144421

19. Xu ST, Ma YQ, Xu YF, Sun X, Geng BQ, Zheng GH, Dai ZX (2015) Pure dipolar-interacted $CoFe_2O_4$ nanoparticles and their magnetic properties. Mater Res Bull 62:142–147

20. Zan FL, Ma YQ, Ma Q, Xu YF, Dai ZX, Zheng GH, Wu MZ, Li G (2013) Magnetic and impedance properties of nanocomposite $CoFe_2O_4/Co_{0.7}Fe_{0.3}$ and single phase $CoFe_2O_4$ via One-step hydrothermal. J Am Ceram Soc 96:3100–3107

21. Zan FL, Ma YQ, Ma Q, Zheng GH, Dai ZX, Wu MZ, Li G, Sun ZQ, Chen XS (2013) One-step hydrothermal synthesis and characterization of high magnetization $CoFe_2O_4/Co_{0.7}Fe_{0.3}$ nanocomposite permanent magnets. J Alloy Compd 553:79–85

22. Adeela N, Maaz K, Khan U, Karim S, Nisar A, Ahmad M, Ali G, Han XF, Duan JL, Liu J (2015) Influence of manganese substitution on structural and magnetic properties of $CoFe_2O_4$ nanoparticles. J Alloy Compd 639:533–540

23. Geng BQ, Ding ZL, Ma YQ (2016) Unraveling the correlation between the remanence ratio and the dipolar field in magnetic nanoparticles by tuning concentration, moment, and anisotropy. Nano Res 9(9):2772–2781

24. Tartaj P, González-Carreño T, Bomatí-Miguel O, Serna CJ, Bonville P (2004) Magnetic behavior of superparamagnetic Fe nanocrystals confined inside submicron-sized spherical silica particles. Phys Rev B 69:094401

25. Bittova B, Vejpravova JP, Morales MPG, Roca A, Mantlikova A (2012) Relaxation phenomena in ensembles of $CoFe_2O_4$ nanoparticles. J Magn Magn Mater 324:1182–1188

26. Mohapatra J, Mitra A, Bahadur D, Aslam M (2015) Superspin glass behavior of self-interacting $CoFe_2O_4$ nanoparticles. J Alloy Compd 628:416–423

27. Soares JM, Cabral FAO, Araújo JHD, Machado FLA (2011) Exchange-spring behavior in nanopowders of $CoFe_2O_4$-$CoFe_2$. Appl Phys Lett 98:072502

28. Fu JC, Zhang JL, Peng Y, Zhao JG, Tan GG, Mellors NJ, Xie EQ, Han WH (2014) Unique magnetic properties and magnetization reversal process of $CoFe_2O_4$ nanotubes fabricated by electrospinning. Nanoscale 4:3932–3936

29. Saidani M, Belkacem W, Bezergheanu A, Cizmas CB, Mliki N (2015) Surface and interparticle interactions effects on nano-cobalt ferrites. J Alloy Compd 653:513–522

30. Sun X, Ma YQ, Xu YF, Xu ST, Geng BQ, Dai ZX, Zheng GH (2015) Improved magnetic performance at low and high temperatures in non-exchange-coupling $CoFe_2O_4/CoFe_2$ nanocomposites. J Alloy Compd 645:51–56

31. Quesada A, Rubio-Marcos F, Marco JF, Mompean FJ, García-Hernández M, Fernández JF (2014) On the origin of remanence enhancement in exchange-uncoupled $CoFe_2O_4$-based composites. Appl Phys Lett 105:202405

32. Xu ST, Ma YQ, Zheng GH, Dai ZX (2015) Simultaneous effects of surface spins: rarely large coercivity, high remanence magnetization and jumps in the hysteresis loops observed in $CoFe_2O_4$ nanoparticles. Nanoscale 7:6520–6526

33. Huber DL (2005) Synthesis, properties, and applications of iron nanoparticles. Small 5:482–501

34. Bhowmik RN, Vasanthi V, Poddar A (2013) Alloying of Fe_3O_4 and Co_3O_4 to develop $Co_{3x}Fe_{3(1-x)}O_4$ ferrite with high magnetic squareness, tunable ferromagnetic parameters, and exchange bias. J Alloy Compd 578:585–594

35. Kneller EF, Hawig R (1991) The exchange-spring magnet: a new material principle for permanent magnets. IEEE Trans Magnetics 27: 3588–3560

36. Cullity BD (1972) Introduction to magnetic materials. Addison-Wesely Publishing, Reading

37. Lakshmi N, Bhargava H, Venugopalan OPK (2009) Magnetic properties resulting from core-shell interactions in nanosized $Ni_{0.25}Co_{0.25}Zn_{0.5}Fe_2O_4$. Phys Rev B 80:174425

38. Bianco LD, Fiorani D, Testa AM, Bonetti E, Savini L, Signoretti S (2002) Magnetothermal behavior of a nanoscale Fe/Fe oxide granular system. Phys Rev B 66:174418